



RESEARCH LETTER

10.1002/2014GL059239

Key Points:

- Recent expansion of Antarctic sea ice agrees with decreasing Southern Ocean SST
- Southern Ocean surface climate trends reverse sign before and after 1980
- Southern Ocean surface climate shows pronounced multidecadal variability

Supporting Information:

- Readme
- Text S1
- Figure S1
- Table S1

Correspondence to:

T. Fan,
tingting@ucar.edu

Citation:

Fan, T., C. Deser, and D. P. Schneider (2014), Recent Antarctic sea ice trends in the context of Southern Ocean surface climate variations since 1950, *Geophys. Res. Lett.*, 41, 2419–2426, doi:10.1002/2014GL059239.

Received 9 JAN 2014

Accepted 20 MAR 2014

Accepted article online 21 MAR 2014

Published online 4 APR 2014

Recent Antarctic sea ice trends in the context of Southern Ocean surface climate variations since 1950

Tingting Fan¹, Clara Deser¹, and David P. Schneider¹¹NCAR, Boulder, Colorado, USA

Abstract This study compares the distribution of surface climate trends over the Southern Ocean in austral summer between 1979–2011 and 1950–1978, using a wide variety of data sets including uninterpolated gridded marine archives, land station data, reanalysis, and satellite products. Apart from the Antarctic Peninsula and adjacent regions, sea surface temperatures and surface air temperatures decreased during 1979–2011, consistent with the expansion of Antarctic sea ice. In contrast, the Southern Ocean and coastal Antarctica warmed during 1950–1978. Sea level pressure (SLP) and zonal wind trends provide additional evidence for a sign reversal between the two periods, with cooling (warming) accompanied by stronger (weaker) westerlies and lower (higher) SLP at polar latitudes in the early (late) period. Such physically consistent trends across a range of independently measured parameters provide robust evidence for multidecadal climate variability over the Southern Ocean and place the recent Antarctic sea ice trends into a broader context.

1. Introduction

Antarctic sea ice extent (SIE) has shown a modest and statistically significant increase since 1979, the period when continuous satellite measurements are available [Parkinson and Cavalieri, 2012]. This modest expansion, evident in all months of the year, is the result of the near cancelation of ice loss in the Bellingshausen and Amundsen Seas, and ice gain in the Ross and Weddell Seas and along the coast of East Antarctica [Cavalieri and Parkinson, 2008; Comiso and Nishio, 2008]. The increase in Antarctic SIE is in stark contrast to the dramatic decrease in Arctic SIE over the same time period [Cavalieri and Parkinson, 2012]. Like the Arctic, Antarctic SIE has shown the largest percentage change in late summer and early fall since the satellite era [Turner et al., 2013].

While the decline in Arctic sea ice has been attributed, at least in part, to rising anthropogenic greenhouse gas (GHG) concentrations [Holland et al., 2006; Screen and Simmonds, 2010], the cause of the overall increase in Antarctic SIE remains a matter of debate. Several mechanisms have been proposed, with contributions from both anthropogenic and natural (internal to the climate system) factors. Aiken and England [2008] and Bintanja et al. [2013] proposed that the increase in melt water flux from the Antarctic continent [Rignot et al., 2013] promotes sea ice expansion by stabilizing the upper portion of the water column. On the other hand, Holland and Kwok [2012] linked observed ice drift and concentration trends during April–September to changes in zonal and meridional near-surface winds. The role of winds was further investigated in the ice-ocean modeling study of Zhang [2013] who found that the observed westerly wind intensification increased sea ice volume by enhancing ridge-ice production, making the ice more resilient to melting. In an earlier study, Zhang [2007] found that warmer temperatures, while decreasing ice growth, can lead to an overall sea ice increase if ice melt is reduced by increased upper ocean stratification and suppressed oceanic heat transport. However, this effect is smaller than the wind effect [Zhang, 2013].

The role of strengthened westerly winds in response to stratospheric ozone depletion and increased GHG was investigated in a coupled model context by Sigmond and Fyfe [2010] and Bitz and Polvani [2012]. Unlike the one-way-forced simulations of Zhang [2013], these coupled modeling studies found a reduction in Antarctic SIE. However, as pointed out by Marshall et al. (The ocean's role in polar climate change: Asymmetric Arctic and Antarctic responses to greenhouse gas and ozone forcing, submitted to *Philosophical Transactions A of the Royal Society*, 2013), the transient and equilibrium responses of the Southern Ocean to an abrupt increase in surface westerlies are of opposite sign, with upper ocean mixed layer processes dominating the near-term response and slow dynamical adjustment of the meridional overturning circulation responsible for the equilibrium response. Regardless of the sign of the response, all of these studies reported a close

relationship between SIE and sea surface temperature (SST) whereby sea ice gain is associated with lower SSTs and vice versa.

The purpose of this observational study is to place the recent Antarctic sea ice trends into a broader environmental and temporal context. We first examine the relationships among Antarctic sea ice concentration, Southern Ocean SST, surface air temperature (SAT), sea level pressure (SLP), and surface zonal wind (U) trends over the period 1979–2011 using uninterpolated gridded surface marine data sets, land station archives, atmospheric reanalysis, and satellite products. We then extend our analysis of Southern Ocean climate trends back to earlier decades (1950–1978) to illustrate the low-frequency behavior of surface climate trends over the Southern Ocean. The data sets and methods are given in section 2. Results are presented in section 3. A discussion and summary are provided in section 4.

2. Data and Methods

The following monthly datasets are used:

1. Sea ice concentration (SIC) based on satellite passive microwave retrievals using the “bootstrap v2” algorithm [Comiso and Nishio, 2008] on a 25×25 km grid for the period 1979–2011, obtained from the National Snow and Ice Data Center.
2. SST from Hadley Center SST version 3 (HadSST3) [Kennedy *et al.*, 2011a, 2011b] and ERA-Interim (ERA-I) Reanalysis [Dee *et al.*, 2011]. The HadSST3 data set, on a $5^\circ \times 5^\circ$ latitude-longitude grid, is based on version 2.5 of the International Comprehensive Ocean-Atmosphere Data Set (ICOADS) but employs different quality control and bias adjustment procedures; the data are neither interpolated nor variance adjusted (e.g., no spatial or temporal smoothing or interpolation, and missing grid boxes are not filled in). ERA-I SST are based on a succession of different products, including the NCEP two-dimensional variational data assimilation until June 2001, the Optimum Interpolation Sea Surface Temperature version 2 product from July to December 2001, the NCEP real-time global daily SST analysis from January 2002 to January 2009, and the operational sea surface temperature and sea ice analysis starting February 2009.
3. SLP and near-surface zonal wind (U) data from ERA-I and from ICOADS Release 2.5 [Woodruff *et al.*, 2011] on a $2^\circ \times 2^\circ$ latitude-longitude grid. Like HadSST3, the ICOADS is based on ship and buoy measurements and contains no spatial or temporal smoothing or infilling. We regrid the $2^\circ \times 2^\circ$ ICOADS data to the $5^\circ \times 5^\circ$ HadSST3 grid using simple bilinear interpolation.
4. Land station SLP and SAT from the Reference Antarctic Data for Environment Research (READER; <http://www.antarctica.ac.uk/met/READER/surface/stationpt.html>) and International Surface Pressure Databank (ISPD; provided by Doctor Xuangang Yin from the National Climatic Data Center) archives.

Changes in observing practice and instrumentation have caused a spurious increase in scalar wind speed since 1950 [Ward and Hoskins, 1996; Norris, 1999; Wu and Xie, 2003; Norris, 2005]. Following the recommendations of Norris [2005; see also Deser and Phillips, 2006], we account for this spurious increase by removing a 4.7% per decade linear trend from the ICOADS wind components. Zonal wind trend patterns from the wave- and anemometer-based sea surface wind (WASWIND) data set [Tokinaga and Xie, 2011] show good agreement with those based on ICOADS (not shown).

We compute seasonal anomalies from the monthly anomalies, requiring a minimum of 1 month per 3 month season. We calculate linear trends from the seasonal anomalies using the method of least squares and assess their statistical significance using a Student's *t* test and taking into account serial autocorrelation based on the method of Zwiers and von Storch [1995]. For the observational archives that contain substantial amounts of missing data (e.g., HadSST3 and ICOADS), at least 50% of the years during 1950–2011 were required to have data at a given grid box and season to compute a trend; otherwise, the trends were set to missing.

3. Results

3.1. Seasonal Trends During 1979–2011

Seasonal and annual trend maps of SIC, SST, and near-surface wind components over the Southern Ocean during 1979–2011 are shown in Figure 1. The SST and wind data are from ERA-I. Cooling is evident over most of the Southern Ocean in all seasons and the annual mean, with magnitudes approximately 0.2 – 0.4°C per decade or 0.7 – 1.3°C over the 33 year period. Two regions of warming stand out within the domain that is otherwise

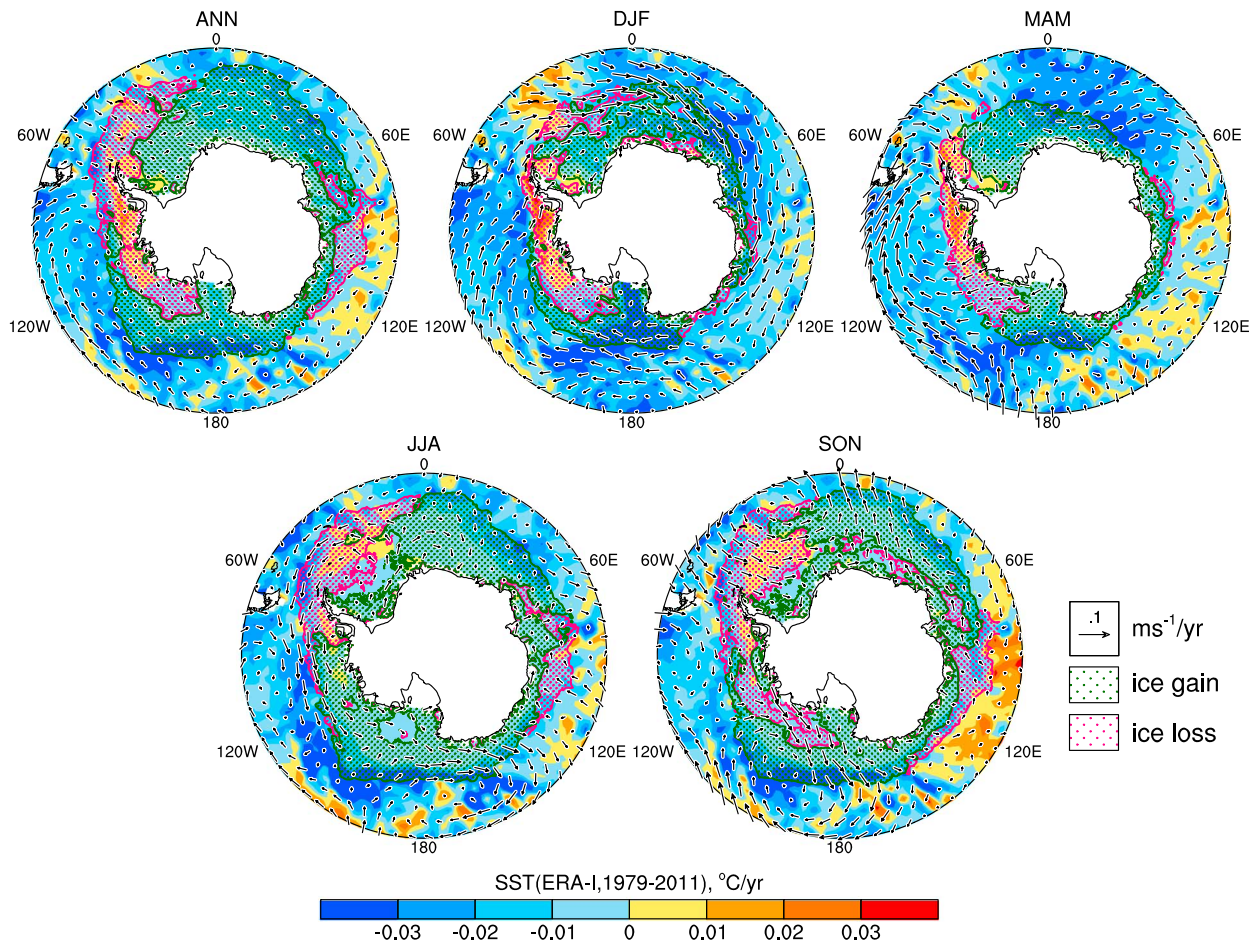


Figure 1. Annual and seasonal trends during 1979–2011 of sea ice concentration (green and magenta stippling for ice gain and ice loss, respectively), SST (color shading, °C/yr), and near-surface winds (vectors, $\text{m s}^{-1} \text{yr}^{-1}$). See text for data sources.

cooling: the Antarctic Peninsula and adjacent Weddell, Bellingshausen and Amundsen Seas, and the sector 80° – 130° E particularly in austral spring (September, October, and November (SON)). Sea ice concentration (SIC) trends are generally consistent with the SST trends: that is, regions of increasing SIC are nearly always found in an environment of decreasing SST, and vice versa. (For visual clarity, we only discriminate the sign of the SIC trends in Figure 1: their magnitudes are shown in Figure 3.) The correspondence between the signs of the SST and SIC trends is a feature of every season and the annual mean.

Wind vector trends show less consistency from season to season than either SST or SIC trends (Figure 1). For example, austral summer (December, January, and February (DJF)) exhibits predominantly westerly wind trends over most of the Southern Ocean, whereas the other seasons show more regional circulation trend patterns that include pronounced meridional wind changes (for example, the cyclonic circulation trend over the eastern Pacific sector in MAM and the anticyclonic circulation trend over the Atlantic sector in SON). The relationship between the wind trends and the SIC and SST trends is complex and varies from season to season. However, regions of enhanced poleward flow (e.g., warm air advection) generally correspond to areas of SST increase and sea ice loss, and vice versa. A particularly clear example is evident in SON, which shows enhanced poleward flow in the western Atlantic sector where there has been a loss of sea ice and warming of the surface ocean, and enhanced equatorward winds in the region of sea ice gain and SST decrease in the East Antarctic sector. The importance of meridional wind anomalies in causing SST anomalies over the Southern Ocean via turbulent heat exchange is consistent with *Sallee et al.* [2010]. Enhanced westerly winds are generally associated with increased sea ice and decreased SST, particularly in DJF, MAM, and the annual mean. As discussed in *Hall and Visbeck* [2002] among others, stronger westerlies increase Ekman transport of cold surface waters

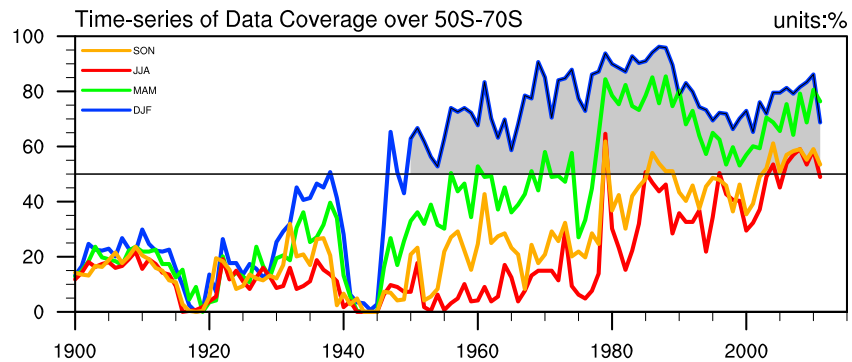


Figure 2. Time series of HadSST3 data coverage over the Southern Ocean (50°S – 70°S) during 1900–2011 stratified by season, expressed as a percentage of grid boxes with at least one observation per season. Only austral summer (DJF; blue curve) contains $>50\%$ continuous data coverage since 1950 (shading).

northward; the resulting divergent Ekman flow near the Antarctic continent advects sea ice farther north leading to an increase in sea ice cover. The annual mean trend distributions in all three fields resemble those in DJF but with reduced magnitude.

3.2. Extending the Record Back to 1950: Data Coverage Over the Southern Ocean

Although the sea ice record cannot be reliably reconstructed before the satellite era, the ship-based HadSST3 and ICOADS data offer the possibility of extension to earlier decades. Figure 2 shows the HadSST3 data coverage over the Southern Ocean (50° – 70°S), expressed as a percentage of grid boxes with at least 1 month of data per season, during the period 1900–2011. Data coverage is scarce in all seasons before about World War II. After 1950, more than 50% of grid boxes contain measurements in austral summer (DJF). The 50% data coverage threshold is reached around 1980 in austral fall (MAM), and not until approximately 2005 in austral winter (JJA) and spring (SON). Similar data sampling is found for the ICOADS variables (SLP, SST, and wind; not shown). Based on these results, and to avoid confusion by sampling different months in different years, we have chosen to limit our subsequent analysis to the season that provides the greatest data coverage (DJF) back to 1950. However, similar results are obtained if we consider all months of the year and if we vary our data coverage threshold to between 30% and 70% (not shown). We emphasize that although our sampling criterion is lenient, we rely on physical consistency among independent climate data sets to assess the reality and robustness of the results.

3.3. Surface Climate Trends: 1979–2011 Versus 1950–1978

Figure 3 compares the distribution of DJF surface climate trends over the Southern Ocean between the periods 1979–2011 and 1950–1978, based on a variety of uninterpolated gridded data sets (SST from HadSST3 and SLP and U from ICOADS), in addition to land station records (SAT from READER; most of SLP data are taken from READER, except three stations along the midlatitude are from ISPD). The SIC trends for the later period are also shown. Note that the color bar for the U trends is reversed to facilitate visual comparison with the SLP and SST trends. Focusing first on the period 1979–2011 (Figures 3d–3g), the widespread cooling of SSTs in the Southern Ocean, except in the region adjacent to the Antarctic Peninsula and nearby seas, is confirmed by ubiquitous cooling in the SAT station data along the coast of East Antarctica (filled circles) and agrees well with the increasing SIC. Likewise, the SST warming in the sector 180° – 30°W adjacent to the Antarctic coast is verified by increasing SAT at land stations and by decreasing SIC. We emphasize that the three data sets (HadSST3, land station SAT, and SIC) are completely independent: their agreement thus provides robust evidence for the reality of the trends. North of $\sim 50^{\circ}\text{S}$, SSTs and land station SAT show a warming trend, except in the far eastern Pacific.

Moving on to the atmospheric variables, we find good correspondence between the U and SLP trends over the Southern Ocean in the recent period, with a general strengthening of the westerlies at high latitudes, in agreement with the lowering of SLP along the Antarctic coast and raising of SLP to the north. Land station data (filled circles) confirm the marine SLP trends. The wind and SLP trends are noisier than their SST counterparts, underscoring the importance of physical consistency to assess the robustness of the atmospheric circulation trends.

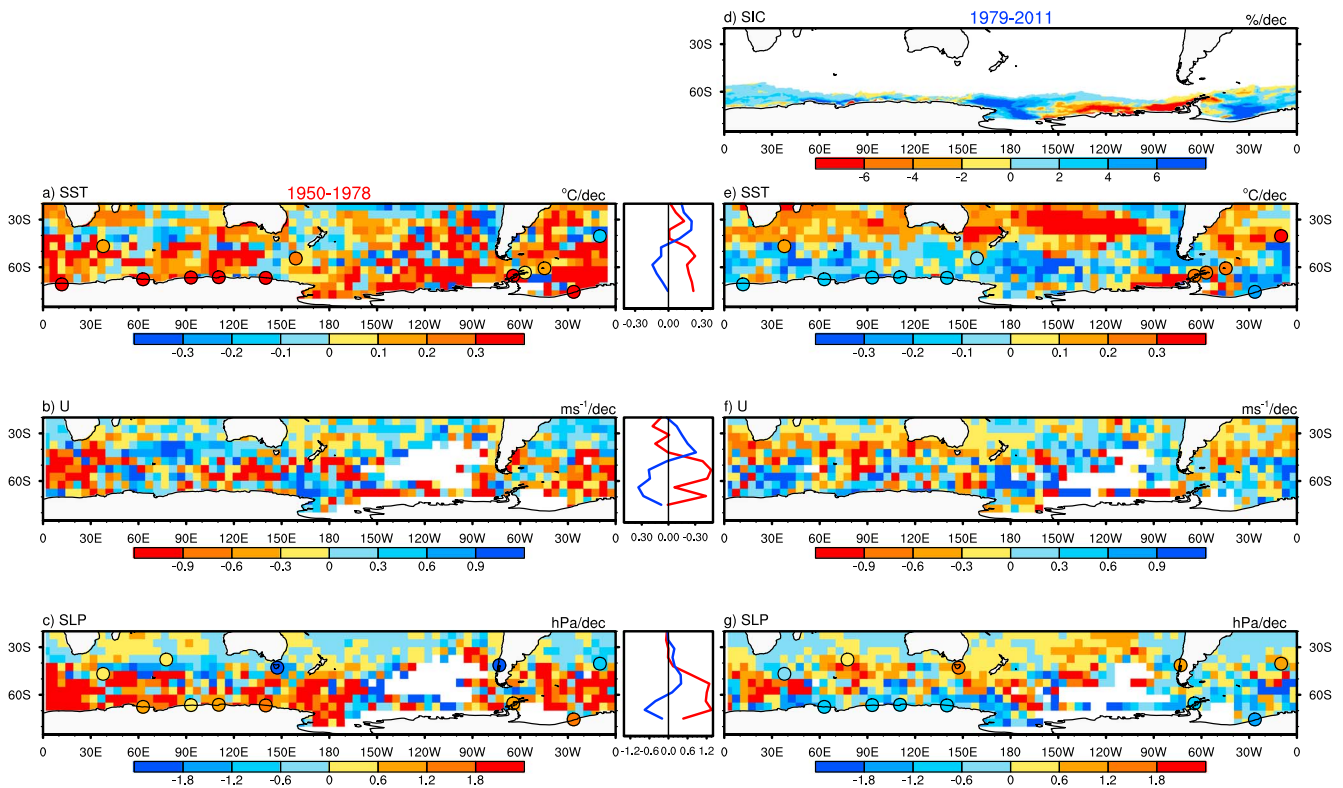


Figure 3. Comparison of austral summer (DJF) surface climate trends during 1950–1978 (left column) and 1979–2011 (right column) and their zonal means (middle column). (a and e) Gridded SST trends ($^{\circ}\text{C}$ per decade) with land station SAT trends ($^{\circ}\text{C}$ per decade) superimposed as colored circles; the same color bar is used for both SST and SAT. (b and f) Zonal wind (U) trends (m s^{-1} per decade); note that the color bar is inverted to facilitate comparison with the other climate variables. (c and g) Gridded marine SLP trends (hPa per decade) with land station SLP trends superimposed as colored circles; the same color bar is used for both. White areas indicate insufficient data coverage for computing trends ($> 60\%$ of the years have missing data for the period indicated). (d) Sea ice concentration (SIC) trends ($\%$ per decade). The middle columns show zonally averaged trends for 1950–1978 (red curves) and 1979–2011 (blue curves) based on the marine data sets. See text for data sources.

Trends based on the uninterpolated ship archives (HadSST3 and ICOADS) for the period 1979–2011 show more grid-scale noise than those based on ERA-I, as expected given that they are not assimilated data products (Figure S1 in the supporting information). However, their agreement with ERA-I in terms of the large-scale patterns is encouraging and lends confidence to their utility for the purpose of this study. These conventional data sets provide the “raw input” to any reanalysis product and that physical consistency amongst the independently measured climate variables in these archives constitutes a strong test of the reality of the trends.

Comparing surface climate trends over the earlier period 1950–1978 with those over the later period 1979–2011 reveals a general reversal in sign (Figures 3a–3c). In particular, the early period shows warming throughout the Southern Ocean, an aspect that is confirmed by the land station SAT data. This warming trend is accompanied by a general decrease in the surface westerlies and by an increase in SLP at high latitudes and decrease at lower latitudes, a pattern confirmed by the SLP station data. In addition to the sign reversal, the early period trends extend farther north than the late period trends. For example, the high-latitude SST warming (cooling) trend during 1950–1978 (1979–2011) extends to $\sim 40^{\circ}\text{S}$ (50°S), and the high-latitude SLP increase (decrease) during 1950–1978 (1979–2011) extends to $\sim 40^{\circ}\text{S}$ ($\sim 60^{\circ}\text{S}$), with the strongest meridional gradient in the latitude band 40° – 50°S (50° – 70°S). This equatorward shift of the strongest gradient in the meridional SLP trends is roughly consistent with that of the maximum amplitude of the zonal wind trends, although the data are noisy. Zonally averaged profiles confirm the sign reversal and sight northward expansion of the trends in the early period compared to the later period (middle column of Figure 3).

3.4. Southern Ocean Time Series

Complementary to the spatial information given in Figure 3, Figure 4 shows zonally averaged DJF time series of Antarctic sea ice extent (SIE) and Southern Ocean SST, U, SLP, and SAT during 1950–2011, expressed as standardized

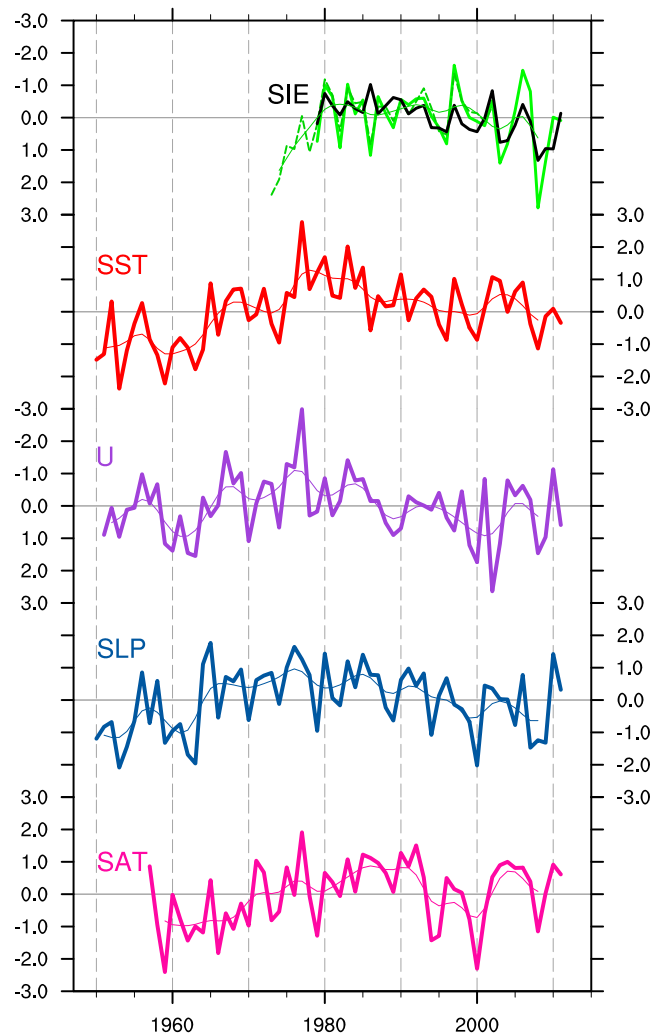


Figure 4. Selected zonally averaged time series, from top to bottom: Antarctic SIE, Southern Ocean (50°–70°S) SST, Southern Ocean (50°–70°S) zonal wind (U), high-latitude SLP (55°–80°S), and Antarctic SAT. Note that the SIE and U records are inverted. The green (black) SIE curve is based on DJF (annual) means, and the dashed green curve denotes an extension of the DJF SIE record back to 1973 based on visual satellite imagery [Cavalieri *et al.*, 2003]; all remaining curves are DJF averages. Thick (thin) curves are based on unsmoothed (12 year low-pass-filtered) data. All records are normalized by dividing by their standard deviation.

anomalies. Low-pass-filtered versions of these records are also shown, using a Gaussian filter (five applications of a three-point binomial filter) that has a half-power point at approximately 12 years. The annual mean (January–December) SIE is also shown, along with a longer record of DJF SIE based on visual satellite imagery that begins in 1973 [Cavalieri *et al.*, 2003]. The SST (HadSST3) and U (ICOADS) records are averaged over the latitude band 50°–70°S, the SLP record (ICOADS) is averaged over 55°–80°S, and the SAT record (which is limited to the period 1957–2011) is the average of all stations south of 50°S (e.g., nine Antarctic records plus Macquarie Island (54.5°S, 158.9°E; the three stations clustered along the Antarctic Peninsula were first averaged together and then combined with the remaining seven SAT records so as not to give undue influence to this region in the Antarctic-wide average)). Note that the SIE and U records have been inverted to facilitate comparison with the other time series.

All five independent climate records show generally similar and physically consistent low-frequency behavior, with upward trends from approximately 1950 to 1978, downward trends from approximately 1979 to 2000, and flat trends thereafter. All trends during both periods are significant at the 95% confidence level taking into account serial autocorrelation, except U in the early period which is significant at the 93% level (Table S1). These low-frequency variations are superimposed upon large interannual fluctuations. Although the reliability of the SIE record before 1979 is questionable, the decrease in SIE during the decade of the 1970s is physically consistent with the simultaneous warming seen in the SST record, lending some confidence to its qualitative reliability.

To quantify the strength of the relationships amongst the time series shown in Figure 4, we have computed correlation coefficients between all pairs of records based on the period 1950–2011 (those with SIE are limited to 1979–2011; Table 1). All correlations are significant at the 95% confidence level taking into account serial autocorrelation, except for SIE with U and SAT which are significant at the 90% level; similar results are found for detrended data (not shown). Antarctic SIE exhibits a negative correlation with Southern Ocean SST ($r = -0.56$), consistent with the trend maps discussed above. Southern Ocean SSTs in turn show positive correlations with high-latitude SLP ($r = 0.63$) and Antarctic SAT ($r = 0.59$), and a negative correlation with Southern Ocean zonal wind ($r = -0.49$). Zonal wind and SLP are highly correlated ($r = 0.66$), confirming the reliability of these records

Table 1. Correlation Coefficients Amongst the Time Series Shown in Figure 4^a

	SIE	SST	U	SLP	SAT
SIE		-0.56	0.31	-0.38	-0.33
SST			-0.49	0.63	0.59
U				-0.66	-0.37
SLP					-0.55

^aValues in plain (bold) font are significant at the 90% (95%) level.

over the past 62 years. Collectively, the overall agreement amongst the independent data sets, both in terms of spatial pattern and temporal variability (Figures 3 and 4), provides compelling evidence for a reversal in sign of Southern Ocean climate trends during the late 1970s to early 1980s.

4. Summary and Discussion

We have evaluated surface climate trends over the Southern Ocean for two periods, 1979–2011 and 1950–1978, using a variety of data sources including uninterpolated ship archives, land station data, and for the later period, ERA-I reanalysis and satellite products. In addition, we have placed the recent trends in Antarctic sea ice concentration into the broader environmental context of Southern Ocean surface climate trends. We focused on austral summer (DJF) when data coverage over the Southern Ocean in the presatellite era is greatest.

During the later period, the distribution of SST trends shows notable and widespread cooling over Southern Ocean, except for the area near the Antarctic Peninsula and adjacent West Antarctica where SST warming is observed. The widespread SST decreases correspond to areas of sea ice expansion, while the region of SST warming is associated with sea ice loss. Such a physically intuitive relationship suggests that SSTs can be used as a proxy for sea ice in areas near the Antarctic continent, allowing inferences of past sea ice behavior from conventional SST measurements. For the Southern Ocean as a whole, SST has decreased by approximately 0.6°C in DJF (0.4°C in the annual mean) while Antarctic SIC has increased by approximately 9% in DJF (12% in the annual mean) during 1979–2011. The surface cooling of the Southern Ocean since 1979 is accompanied by intensified westerly winds and a strengthened meridional SLP gradient, both in DJF and in the annual mean.

All data sets (SST, SAT, SLP, and U) show a consistent reversal in sign of the Southern Ocean surface climate trends between 1979–2011 and 1950–1978. The independence of the various data sets provides strong evidence for the reality of the trend reversal. Early satellite records of Antarctic SIE collected from the Nimbus 5 electrically scanning microwave radiometer during 1973–1979, although of questionable reliability, also show a reversal in sign before 1979, suggesting they are at least qualitatively plausible. In addition to the sign reversal, the meridional extent of the Southern Ocean surface climate trends shows a consistent northward expansion of approximately 10° of latitude during 1950–1978 compared to 1979–2011 in all data sets. Such physically consistent trends across a range of independently measured climate parameters provide a broader context for the recent increase in Antarctic sea ice. We note that similar low-frequency fluctuations during the past 50 years have been found in surface air temperature records [Turner *et al.*, 2005; Jacka *et al.*, 2004], sea level pressures [Turner *et al.*, 2005], and in ice core-based proxy temperature records [Schneider *et al.*, 2006].

The mechanisms underlying the low-frequency surface climate trends over the Southern Ocean identified in this study remain to be addressed. As mentioned in section 1, intensified surface westerly winds driven in part by stratospheric ozone depletion and GHG increase may be responsible for the surface cooling and sea ice expansion since 1979 [Zhang, 2013]. However, coupled models participating in the Coupled Model Intercomparison Project phase 5 (CMIP5) [Turner *et al.*, 2013] generally do not simulate SST cooling nor sea ice expansion over the high-latitude Southern Hemisphere [Polvani and Smith, 2013], suggesting that decadal-scale climate variability may also be a factor. The reversal of the sign of the trends before and after about 1980 also suggests the importance of internally generated variability. While the general sign reversal of the trends may be viewed as a response to stratospheric ozone depletion, it could also be viewed in the context of low-frequency variability generated by tropical dynamics [e.g., Okumura *et al.*, 2012; Schneider and Noone, 2012]. The additional context for observed trends provided here will help guide future work, aimed at understanding the proximate causes for the spatial patterns and temporal evolution of surface climate trends over the Southern Ocean since 1950.

Acknowledgments

We acknowledge helpful discussions with Lorenzo M. Polvani, Yuko Okumura, and Ana Ordonez (who provided additional contextual analyses) during the course of this study. We are grateful to Donald Cavalieri for sharing the Antarctic sea ice extent record for the period 1973 to 2002 and to Xungang Yin for supplying the station data at Puerto Montt, Christchurch, Hobart and Ile Nouvelle-Amsterdam. We also thank the two anonymous reviewers for their thoughtful comments and suggestions. The figures were produced with the NCAR Command Language (NCL) software package. Tingting Fan is supported by the China Scholarship Council (CSC). David Schneider is supported by National Science Foundation (NSF) grants 1048899 and 1235231. NCAR is sponsored by the NSF.

The Editor thanks two anonymous reviewers for their assistance in evaluating this paper.

References

- Aiken, C. M., and M. H. England (2008), Sensitivity of present-day climate to freshwater forcing associated with Antarctic sea ice loss, *J. Clim.*, *21*, 3936–3946, doi:10.1175/2007JCLI1901.1.
- Bintanja, R., G. J. van Oldenborgh, S. S. Drijfhout, B. Wouters, and C. A. Katsman (2013), Important role for ocean warming and increased ice-shelf melt in Antarctic sea-ice expansion, *Nat. Geosci.*, *6*, 376–379, doi:10.1038/ngeo1767.
- Bitz, C. M., and L. M. Polvani (2012), Antarctic climate response to stratospheric ozone depletion in fine resolution ocean climate model, *Geophys. Res. Lett.*, *39*, L20705, doi:10.1029/2012GL053393.
- Cavalieri, D. J., C. L. Parkinson, and K. Y. Vinnikov (2003), 30-year satellite record reveals contrasting Arctic and Antarctic decadal sea ice variability, *Geophys. Res. Lett.*, *30*(18), 1970, doi:10.1029/2003GL018031.
- Cavalieri, D. J., and C. L. Parkinson (2008), Antarctic sea ice variability and trends, 1979–2006, *J. Geophys. Res.*, *113*, C07004, doi:10.1029/2007JC004564.
- Cavalieri, D. J., and C. L. Parkinson (2012), Arctic sea ice variability and trends, 1979–2010, *Cryosphere*, *6*, 881–889, doi:10.5194/tc-6-881-2012.
- Comiso, J. C., and F. Nishio (2008), Trends in the sea ice cover using enhanced and compatible AMSR-E, SSM/I, and SMMR data, *J. Geophys. Res.*, *113*, C02507, doi:10.1029/2007JC004257.
- Dee, D. P., et al. (2011), The ERA-Interim reanalysis: Configuration and performance of the data assimilation system, *Q. J. R. Meteorol. Soc.*, *137*, 553–597, doi:10.1002/qj.828.
- Deser, C., and A. S. Phillips (2006), Simulation of the 1976/1977 climate transition over the North Pacific: Sensitivity to tropical forcing, *J. Clim.*, *19*, 6170–6180, doi:10.1175/JCLI3963.1.
- Hall, A., and M. Visbeck (2002), Synchronous variability in the Southern Hemisphere atmosphere, sea ice, and ocean resulting from the annular mode, *J. Clim.*, *15*, 3043–3057.
- Holland, M. M., C. M. Bitz, and B. Tremblay (2006), Future abrupt reductions in the summer Arctic sea ice, *Geophys. Res. Lett.*, *33*, L23503, doi:10.1029/2006GL028024.
- Holland, P. R., and R. Kwok (2012), Wind-driven trends in Antarctic sea-ice drift, *Nat. Geosci.*, *5*, 872–875, doi:10.1038/ngeo1627.
- Jacka, T. H., W. F. Budd, and A. Holder (2004), A future assessment of surface temperature changes at stations in the Antarctic and Southern Ocean, 1949–2002, *Ann. Glaciol.*, *39*, 331–338.
- Kennedy, J. J., N. A. Rayner, R. O. Smith, D. E. Parker, and M. Saunby (2011a), Reassessing biases and other uncertainties in sea surface temperature observations measured in situ since 1850: 1. Measurement and sampling uncertainties, *J. Geophys. Res.*, *116*, D14103, doi:10.1029/2010JD015218.
- Kennedy, J. J., N. A. Rayner, R. O. Smith, D. E. Parker, and M. Saunby (2011b), Reassessing biases and other uncertainties in sea surface temperature observations measured in situ since 1850: 2. Biases and homogenisation, *J. Geophys. Res.*, *116*, D14104, doi:10.1029/2010JD015220.
- Norris, J. R. (1999), On trends and possible artifacts in global ocean cloud cover between 1952 and 1995, *J. Clim.*, *12*, 1864–1870.
- Norris, J. R. (2005), Trends in upper-level cloud cover and surface divergence over the tropical Indo-Pacific Ocean between 1952 and 1997, *J. Geophys. Res.*, *110*, D21110, doi:10.1029/2005JD006183.
- Okumura, Y., D. P. Schneider, and C. Deser (2012), Decadal-interdecadal climate variability over Antarctica and linkages to the tropics: Analysis of ice core, instrumental, and tropical proxy data, *J. Clim.*, *25*, 7421–7441.
- Parkinson, C. L., and D. J. Cavalieri (2012), Antarctic sea ice variability and trends, 1979–2010, *Cryosphere*, *6*, 871–880, doi:10.5194/tc-6-871-2012.
- Polvani, L. M., and K. L. Smith (2013), Can natural variability explain observed Antarctic sea ice trends? New modeling evidence from CMIP5, *Geophys. Res. Lett.*, *40*, 3195–3199, doi:10.1002/grl.50578.
- Rignot, E., S. Jacobs, J. Mouginot, and B. Scheuchl (2013), Ice-shelf melting around Antarctica, *Science*, *319*, 266–270, doi:10.1126/science.1235798.
- Schneider, D. P., E. J. Steig, T. D. Van Ommen, D. A. Dixon, P. A. Mayewski, J. M. Jones, and C. M. Bitz (2006), Antarctic temperatures over the past two centuries from ice cores, *Geophys. Res. Lett.*, *33*, L16707, doi:10.1029/2006GL027057.
- Schneider, D. P., and D. C. Noone (2012), Is a bipolar seesaw consistent with observed Antarctic climate variability and trends?, *Geophys. Res. Lett.*, *39*, L06704, doi:10.1029/2011GL050806.
- Sallee, J. B., K. G. Speer, and S. R. Rintoul (2010), Zonally asymmetric response of the Southern Ocean mixed-layer depth to the southern annular mode, *Nat. Geosci.*, *3*, 273–279, doi:10.1038/NNGEO812.
- Screen, J. A., and I. Simmonds (2010), The central role of diminishing sea ice in recent Arctic temperature amplification, *Nature*, *464*, 1334–1337, doi:10.1038/nature09051.
- Sigmond, M., and J. C. Fyfe (2010), Has the ozone hole contributed to increased Antarctic sea ice extent?, *Geophys. Res. Lett.*, *37*, L18502, doi:10.1029/2010GL044301.
- Tokinaga, H., and S. P. Xie (2011), Wave- and anemometer-based sea surface wind (WASWind) for climate change analysis, *J. Clim.*, *24*, 267–285, doi:10.1175/2010JCLI3789.1.
- Turner, J., S. R. Colwell, G. J. Marshall, T. A. Lachlan-Cope, A. M. Carleton, P. D. Jones, V. Lagun, P. A. Reid, and S. Iagovkina (2005), Antarctic climate change during the last 50 years, *Int. J. Climatol.*, *25*, 279–294, doi:10.1002/joc.1130.
- Turner, J., T. Bracegirdle, T. Phillips, G. J. Marshall, and J. S. Hosking (2013), An initial assessment of Antarctic sea ice extent in the CMIP5 models, *J. Clim.*, *26*, 1473–1484, doi:10.1175/JCLI-D-12-00068.1.
- Ward, M. N., and B. J. Hoskins (1996), Near-surface wind over the global ocean 1949–1988, *J. Clim.*, *9*, 1877–1895.
- Woodruff, S. D., et al. (2011), ICOADS release 2.5: Extensions and enhancements to the surface marine meteorological archive, *Int. J. Climatol.*, *31*, 951–967, doi:10.1002/joc.2013.
- Wu, R., and S. P. Xie (2003), On equatorial Pacific surface wind changes around 1977: NCEP–NCAR reanalysis versus COADS observations, *J. Clim.*, *16*, 167–173.
- Zhang, J. (2007), Increasing Antarctic sea ice under warming atmospheric and oceanic conditions, *J. Clim.*, *20*, 2515–2529, doi:10.1175/JCLI4136.1.
- Zhang, J. (2013), Modeling the impact of wind intensification on Antarctic sea ice volume, *J. Clim.*, *27*, 202–214, doi:10.1175/JCLI-D-12-00139.1.
- Zwiers, F. W., and H. von Storch (1995), Taking serial correlation into account in tests of the mean, *J. Clim.*, *8*, 336–351.